Chiang Mai J. Sci. 2017; 44(3) : 1091-1099
http://epg.science.cmu.ac.th/ejournal/
Contributed Paper

Physicochemical Properties of Magnesium-doped Hydroxyapatite Nanoparticles Prepared by Incipient Wetness Impregnation Method

Jutharatana Klinkaewnarong [a,d], Sirilak Kamonwannasit [b], Piaw Phatai* [c,d]

[a] Program in Physics, Faculty of Science, Udon Thani Rajabhat University, Udon Thani 41000, Thailand.

[b] Department of Natural Product Technology, Faculty of Agricultural Technology, Burapha University, Sakaeo 27160, Thailand.

[c] Department of Chemistry, Faculty of Science, Udon Thani Rajabhat University, Udon Thani 41000, Thailand.

[d] Polymer and Material Research groups, Faculty of Science, Udon Thani Rajabhat University, Udon Thani 41000, Thailand.

*Author for correspondence; e-mail: piawtee99@hotmail.com

Received: 13 May 2016
Accepted: 19 August 2016

ABSTRACT

Nanocrystalline hydroxyapatite powders are successfully synthesized by sol-gel method with calcination temperature at 600 °C for 2 h. The molar ratio of Ca: P is kept at 1.67 as hydroxyapatite (HAp). Different weight percents of the magnesium-doped hydroxyapatite (xMg/HAp, x = 0, 1, 3, 5, 7 and 9 wt.%) were prepared via incipient wetness impregnation method. The physicochemical properties of the xMg/HAp were investigated by X-ray diffraction (XRD), Energy dispersive X-ray spectroscope (EDX), Transmission electron microscope (TEM), Fourier transform infrared spectroscope (FT-IR) and UV-vis diffuse reflectance spectroscope (UV-vis DRS). The XRD measurement showed that the magnesium ion was homogeneously incorporated into the hexagonal structure of HAp and the lattice parameters, *a* and *c*, are in the ranges of 0.9356-0.9396 and 0.6846-0.6869 nm, respectively. Beta-tricalcium phosphate (β-TCP, $Ca_3(PO_4)_2$) was detected at all compositions and calcium oxide (CaO) was detected with the doped Mg^{2+} greater than 1 wt.%. The EDX analyses showed that the Ca/P molar ratio gradually decreased with increasing amount of Mg, whereas the (Ca+Mg)/P molar ratio increased. The FT-IR and UV-vis DRS techniques confirmed the formation of HAp. Doping of Mg^{2+} up to 5 wt.% resulted in the formation of 68-123 nm particles of spherical shapes, while the spherical and rod-like shapes were obtained at 7 and 9 wt.% Mg^{2+}, with their width of 46 and 75 nm, respectively.

Keywords: hydroxyapatite, impregnation method, magnesium, solid characterization

1. INTRODUCTION

Hydroxyapatite (HAp, $Ca_{10}(PO_4)_6(OH)_2$) is one of the most stable forms of calcium phosphate phases which are the main constituent mineral of bone and the teeth in mammals. It has excellent properties such as bioactivity, osteoconductivity, biocompatibility, etc. [1, 2]. Some of the applications of HAp include injectable bone cements, immediate tooth replacement, bone defect repairing, and pulp capping material. Due to their rather poor mechanical characteristics and brittleness especially in the wet environments [3], the application of HAp ceramics is however limited to the spot not carrying high mechanical loads. Besides, formation of nano-sized HAp has great functional properties owing to its grain size, large surface area and ultra-fine structure similar to biological apatite, which will have a good impact on implant-cell interaction in the body environment [4].

Previous researches have been studied on doped HAp using various metal ions such as Mg^{2+}, Zn^{2+}, La^{3+}, Y^{3+} and In^{3+} for improving orthopedic and dental applications [5, 6]. The incorporation of various inorganic additions into HAp structure in the form of metal ions or inorganic salt anions may facilitate sintering of the material, but it can also significantly affect structural, physico-chemical, mechanical and biological properties of HAp-based materials. Divalent magnesium ion (Mg^{2+}) associated with biological apatite was found to be one of the most important ions because it has an active participation in the synthesis of the biological apatite crystals by promoting bone mineralization and controlling the growth of HAp crystals in in-vivo conditions [7].

In the literature, many approaches were used for synthesis of doped HAp, including co-precipitation [8], sol-gel [9], microwave hydrothermal [10], solid state reaction [11], reverse microemulsion [12] and *in-situ* synthesis [13]. The doped HAp synthesized through incipient wetness impregnation was widely used as a catalyst in catalytic activity [14-16]. However, it has never been reported for use as a biomaterial.

Hence, the purpose of this work was to synthesize the Mg^{2+} ion doped HAp (xMg/HAp, x = 0, 1, 3, 5, 7 and 9% by weight) through the incipient wetness impregnation method. The HAp thus-synthesized were characterized by using X-ray diffraction (XRD), Energy dispersive X-ray spectroscope (EDX), Transmission electron microscope (TEM), Fourier transform infrared spectroscope (FT-IR) and UV-vis diffuse reflectance spectroscope (UV-vis DRS).

2. MATERIALS AND METHODS

2.1 Chemicals and Reagents

Chemical reagents such as calcium nitrate tetrahydrate ($Ca(NO_3)_2{\cdot}4H_2O$, 99.9 wt.%, Kanto Chemical), ammonium hydrogen phosphate ($(NH_4)_2HPO_4$, 99.0 wt.%, BDH), magnesium nitrate hexahydrate ($Mg(NO_3)_2{\cdot}6H_2O$, 99.0 wt.%, UNILAB) and ethanol (C_2H_5OH, 99.7-100%, BDH) were purchased from Merck (Germany). All chemicals were of analytical grade and utilized without further purification. Distilled water was used as a solvent.

2.2 Preparation of Hap and xMg/HAp

The preparation of HAp was carried out by using the sol-gel method similar to that of Sung *et al.* [17]. The molar ratio of Ca/P was kept at 1.67 as HAp. A mixture, composed of $Ca(NO_3)_2{\cdot}4H_2O$ in 100 mL of C_2H_5OH as well as $(NH_4)HPO_4$ in 50 mL of distilled water, was first prepared in a 500 mL-beaker and stirred continuously at room temperature. Then, the mixture was

dried at 100 °C in a hotplate, and finally calcined at 600 °C for 2 h. And the as-synthesized HAp power was obtained.

The xMg/HAp (x = 1, 3, 5, 7 and 9 wt.%) was prepared by the modified incipient wetness impregnation method [18] using $Mg(NO_3)_2 \cdot 6H_2O$ as a precursor. Before the impregnation step, the distilled water was dropped into the weighted amount of dried HAp until the HAp became slightly wet, and the weight/water volume ratio was recorded. The solution of $Mg(NO_3)_2 \cdot 6H_2O$ with desired Mg loading was added dropwise over the HAp, with the mixing of the whole mass as time went on. The mixture was then dried at room temperature overnight and heated at 110 °C for 3 h before its calcination under the condition of 400 °C in air for 3 h. Note that various compositions of xMg/HAp (x = 0, 1, 3, 5, 7 and 9 wt.%) are denoted as HAp, 1Mg/HAp, 3Mg/HAp, 5Mg/HAp, 7Mg/HAp and 9Mg/HAp, respectively.

2.3 Characterization Techniques

Crystal phase identification of HAp and xMg/HAp was analyzed by using an X-ray diffractometer (XRD, D2 Phaser, Bruker, Germany) with an accelerating voltage of 40 kV, current of 35 mA and Cu Kα radiation (λ=1.54184 Å). The weight percentages of Ca, P, O, and Mg and Ca/P ratio were determined by using energy dispersive X-ray (EDX, S-3000N HITACHI). Distribution and diameters of HAp particles were measured by transmission electron microscope (TEM, Ziess, EM902, Germany) with an accelerating voltage of 80 kV. Each sample was dispersed in absolute ethanol, dropped on a carbon-coated copper grid, dried and transferred into the TEM chamber. The functional group of the prepared samples was determined by using Fourier transform infrared spectroscope (FT-IR, Spectrum two-Perkin Elmer) in the spectral range of 500-4000 cm^{-1} in attenuated total reflectance mode. Diffuse reflectance UV-vis spectra (UV-vis DRS) were measured at room temperature using a Lamda 35, Perkin Elmer system equipped with a reflectance attachment which used a $BaSO_4$ coated integration sphere. The measured spectra were treated using Kubelka-Munk functions to compensate for the difference between transmission and reflection measurements.

3. RESULTS AND DISCUSSION

3.1 XRD

Figure 1 shows the XRD patterns of the as-synthesized HAp and xMg/HAp. The XRD patterns of the samples indicate that the major diffraction peaks at $2\theta = 26.5°$, 32.5°, 33.0°, 49.2° and 53.0° can be well indexed to hexagonal-phase $Ca_{10}(PO_4)_6(OH)_2$ when compared with the standard diffraction patterns (JCPDS Card No. 09-0432). The diffraction peaks were sharp and narrow implying that synthesized HAp exhibited high crystallinity. The peaks corresponding to tricalcium phosphate (β-TCP) at $2\theta = 26.5°$ and 30.2° were detected at all compositions and calcium oxide (CaO) at $2\theta = 38.2°$ was detected with the doped Mg^{2+} greater than 1 wt.%. According to Uysal *et al.* [19], the formation of CaO phase can be explained because the Mg^{2+} partially incorporated into HAp hexagonal structure results in the detachment of some Ca^{2+} ions, which form CaO phase.

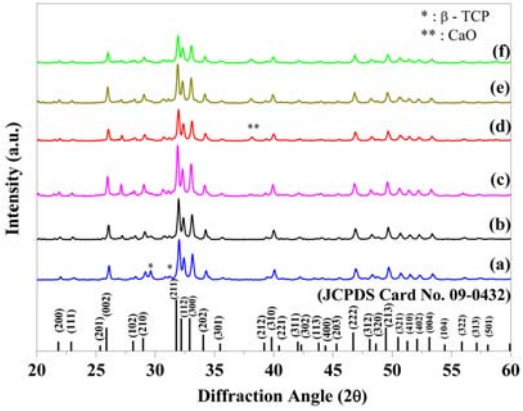

Figure 1. XRD patterns of xMg/HAp samples: (a) pure HAp, (b) 1Mg/HAp, (c) 3Mg/HAp, (d) 5Mg/HAp, (e) 7Mg/HAp, and (f) 9Mg/HAp.

For the general hexagonal crystal system, the relationship between the crystal plane index and interplanar distance (d_{hkl}) is given by the following equation [20]:

$$\frac{1}{d_{hkl}} = \left[\frac{4(h^2+k^2+hk)}{3a^2} + \frac{l^2}{c^2}\right]^{1/2}$$

where h, k and l are the miller indices of the crystal plane. *a* and *c* are the lattice parameter. The average *a* value of the HAp samples was calculated using the plane indices of (100), (200), (210), (300), (310), (320), (410), (420) and (520), while the average *c* value was computed using the plane indices of (002) and (004).

In Table 1, the "*a*" and "*c*" values of the as-synthesized HAp are 0.9356 and 0.6846 nm, respectively which are close to lattice parameters of stoichiometric HAp (JCPDS Card No. 09-0432; a = 0.9418 nm and c = 0.6884 nm). When the Mg^{2+} was incorporated into HAp, the lattice parameter values increased because the ionic radius of Mg^{2+} ion (0.069 nm) is smaller than that of Ca^{2+} ion (0.106 nm). Thus, some Mg^{2+} ions could substitute Ca^{2+} ion in the HAp as well as β-TCP structures. A similar result was reported by Gozalian *et al.* [21] who, in preparing Mg-doped calcium phosphate nanopowders, observed that the presence of Mg^{2+} led to the formation of Mg-doped HAp and Mg- β-TCP. However, there was no significant variation in the lattice parameter values and the volumes of the unit cells of the samples.

For the substitution mechanism, the replacement of Ca^{2+} with other cations in HAp crystalline lattice may be related to the ionic radius, electronegativity and effective charge of the substituting cation compared to those of Ca^{2+}. The lattice of the HAp contains two calcium atoms with different crystal configurations denoted Ca(1) and Ca(2). The Ca(1) atoms occupies the columnar sites and they are nine-fold coordinated. The Ca(2) atoms are located in the channels that pass through the three-dimensional network of the PO_4 tetrahedra and they are seven-fold coordinated [22, 23]. The effective Ca^{2+} ionic radii for seven- and nine-coordination are of 0.106 and 0.118 nm, respectively. This differences in size suggests that Mg^{2+} ions smaller than Ca^{2+} ions should favor the Ca(2) site.

3.2 EDX Analysis

The chemical composition of HAp and xMg/HAp was analyzed by means of large area EDX analysis and the result is depicted in Table 1. It can be observed that the theoretical weight percentages of Ca, P, O and Mg are 39.9, 18.5, 41.4 and 0-9%, respectively. The measured weight percentages of those elements were 11-19, 7-12, 69-75 and 0-8%, respectively. The measured oxygen weight fractions are more than values which should have been measured, almost certainly as due to atmospheric contamination mainly by oxygen and water vapour. This has depressed the determinations of the weight

fractions of Ca, P and Mg. Apart from the problem with oxygen contamination these discrepancies could have been exacerbated by metal loss during the calcination at high temperature. Moreover, few amounts of Mg were detected. This was proven in the XRD measurements, where magnesium oxides were not evident. The Ca/P molar ratio of pristine HAp is 1.60, which is lower than that of the stoichiometric ratio of 1.67. This can be explained that the Ca/P ratio of several particles and aggregates diverged from the stoichiometric ratio of HAp. The possible explanation is owing to the mixture of HAp and other calcium phosphate in the aggregates [24]. The Ca/P molar ratio gradually decreased with increasing amount of Mg, whereas the (Ca+Mg)/P molar ratio increased. These indicated that Mg/HAp powders were more calcium-deficient and thermally unstable than HAp powder. Thus, Mg^{2+} incorporation in HAp promoted formation of β-TCP and reduced the thermal stability of calcium-deficient hydroxyapatite [25]. The decrease of phosphorous in the solid may be associated with the presence of β-TCP phase.

Table 1. Weight percentages of Ca, P, O and Mg in HAp samples derived from EDX.

x% Mg-HAp	Lattice parameters (nm)		% weight				Ca/P Molar ratio	(Ca+Mg)/P Molar ratio
	a	*c*	Ca	P	O	Mg		
0	0.9356	0.6846	18.73	11.69	69.58	0.00	1.60	1.60
1	0.9368	0.6854	17.66	11.89	69.68	0.77	1.48	1.55
3	0.9393	0.6869	15.81	10.75	71.33	2.10	1.47	1.67
5	0.9375	0.6846	14.85	10.09	72.26	2.80	1.47	1.75
7	0.9396	0.6867	13.32	8.84	74.14	3.70	1.51	1.93
9	0.9388	0.6864	11.50	7.65	69.51	7.52	1.50	2.49

3.3 TEM

The TEM images of the pure HAp and xMg/HAp are shown in Figure 2. The morphology of pure HAp particles formed from the ethanol solution (Figure 2a) was in spherical shape, having an average particle size of 110 mm. When the Mg^{2+} ion was impregnated into HAp with the amount of 1, 3 and 5 wt.%, the irregular spherical particles with average particle size of 103, 123 and 68 nm, respectively were obtained. With the 7Mg/HAp, the rod-like shape and spherical particles were observed and its rod width was 46 nm. More aggregated rod particles were observed in 9Mg/HAp, with its rod width of 75 nm. It is observed that the morphology of nanosized HAp particles changing from the spherical to rod-like shapes at 7 and 9 wt.% Mg^{2+}. Such a result was also documented by Sutha *et al.* [22]. The observed structural change is due to the incorporation of magnesium atom into the HAp lattice which promotes the growth direction along one axis and transforms its shape from sphere to rod shape. The nano-sized HAp has a great impact on improving its mechanical properties, allowing for a faster implant surface turnover [23].

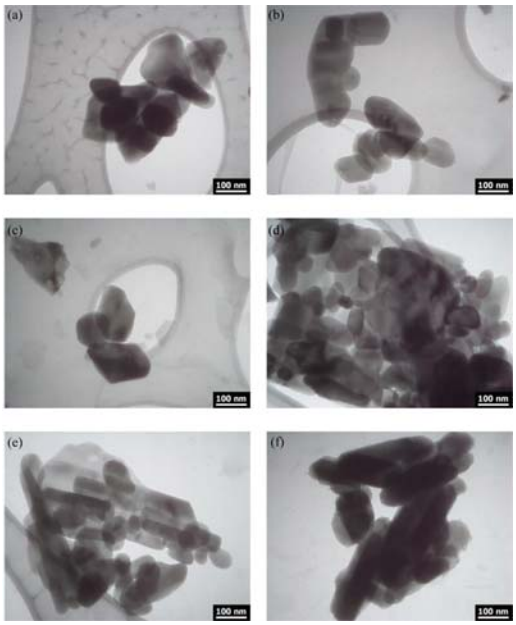

Figure 2. TEM images of xMg/HAp samples: (a) pure HAp, (b) 1Mg/HAp, (c) 3Mg/HAp, (d) 5Mg/HAp, (e) 7Mg/HAp, and (f) 9Mg/HAp.

3.4 FT-IR

The powder FT-IR spectra of the pure HAp and xMg/HAp are illustrated in Figure 3. The sharp bands at 568 and 602 cm^{-1} are assigned to the O-P-O bending modes and the bands positioned at 915-1029 cm^{-1} are ascribed to the phosphate group [11, 26, 27]. The peaks detected at 3141-3570 and 638 cm^{-1} are dispensed to the stretching and bending vibrations of the O-H group, respectively, which indicates the presence of physisorbed water molecules from atmospheric moisture during the measurements [4, 28]. The band at 1681 cm^{-1} is attributed to the adsorbed water. The presence of peaks at 850-900 cm^{-1} in all samples confirms that the samples contain HPO_4^{2-}. The weak peaks located around 1302-1512 cm^{-1} is due to carbonate ion (CO_3^{2-}), which indicates the presence of carbon dioxide adsorbed from atmosphere [29, 30]. The bands detected at 1250-1100, 930, 760 and 530 cm^{-1} showed the formation of mixture phases of HAp and β-TCP. Moreover, the presence of Mg^{2+} in HAp lattice did not change the characteristic peaks of HAp. Thus, the FT-IR spectra of obtained materials verify the formation of HAp.

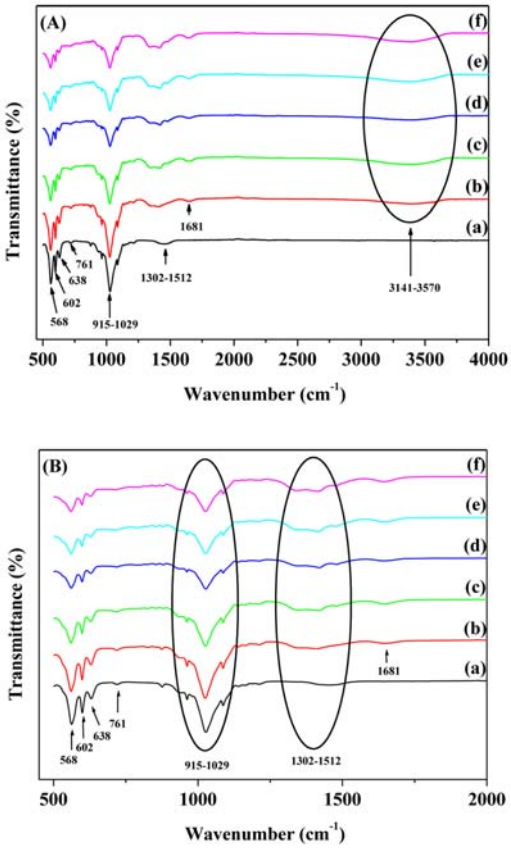

Figure 3. FT-IR of xMg/HAp samples: (a) pure HAp, (b) 1Mg/HAp, (c) 3Mg/HAp, (d) 5Mg/HAp, (e) 7Mg/HAp, and (f) 9Mg/HAp using scan ranges of (A) 500-4000 cm^{-1} and (B) 500-2000 cm^{-1}.

3.5 UV-vis DRS

UV-DR spectroscopy can yield information about the coordination environment and oxidation states of embedded metal ions. Figure 4 illustrates the UV-vis DRS spectra in the range 200-400 nm

of pure HAp and Mg/HAp samples. The peaks at ~230 and 290 nm might be due to the charge transfer transition of $O^{2-} \rightarrow Ca^{2+}$ and $O^{2-} \rightarrow P^{5+}$ of PO_4^{3-} in CaHAp crystal, respectively [31-33].

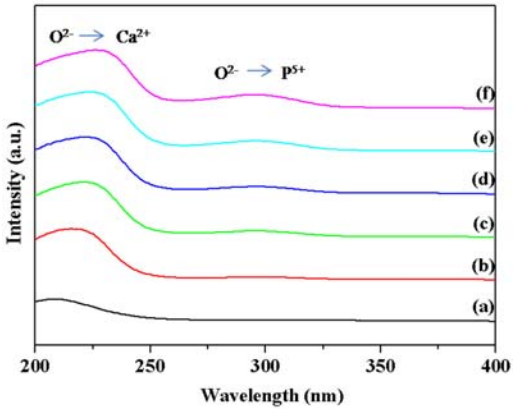

Figure 4. UV-vis DRS spectra of xMg/HAp samples: (a) pure HAp, (b) 1Mg/HAp, (c) 3Mg/HAp, (d) 5Mg/HAp, (e) 7Mg/HAp, and (f) 9Mg/HAp.

4. CONCLUSIONS

Nano-sized Mg/HAp particles were successfully synthesized through the incipient wetness impregnation method. The characterization techniques confirm that the formation of HAp as well as β-TCP and CaO as the second phase is obtained. The Ca/P ratios decrease with the increase of Mg^{2+} loading. Some Mg^{2+} ions could substitute Ca^{2+} ion in the HAp structure. However, there was no significant variation in the lattice parameter values and the volumes of the unit cells of the samples. The morphology of nano-sized HAp particles is changed from the spherical to rod-like shapes at 7 and 9 wt.% Mg^{2+}, which have the rod widths of 46 and 75 nm, respectively. The FT-IR and UV-vis DRS spectra provide good evidence of HAp formation under different studied conditions.

ACKNOWLEDGEMENTS

The authors would like to acknowledge the Department of Chemistry and Department of Physics, Faculty of Science; Research and Development Institute, Udon Thani Rajabhat University, Thailand for their financial support of this research. Many thanks to Prof. Dr. Chih-Hsiang Liao of Department of Environmental Resources Management, Chia-Nan University of Pharmacy and Science for his assistance in proofreading the manuscript.

REFERENCES

[1] Tan F., Naciri M., Dowling D. and Al-Rubeai M., *Biotechnol. Adv.*, 2012; **30**: 352-362. DOI 10.1016/j.biotechadv.2011.07.008.

[2] Roy P. and Sailaja R.R.N., *J. Mech. Behav. Biomed. Mater.*, 2015; **49**: 1-11. DOI 10.1016/j.jmbbm.2015.04.022.

[3] Al-Sanabani J.S., Madfa A.A. and Al-Sanabani F.A., *Int. J. Biomater.*, 2013; 1-12. DOI 10.1155/2013/876132.

[4] Tang C.Y., Uskokovic P.S., Tsui C.P., Veljovic Dj., Petrovic R. and Janackovic Dj., *Ceram. Int.*, 2009; **35**: 2171-2178. DOI 10.1016/j.ceramint.2008.11.028.

[5] Supova M., *Ceram. Int.*, 2015; **41**: 9203-9231. DOI 10.1016/j.ceramint.2015.03.316.

[6] José R., Guerra-López Gustavo A., Echeverría Jorge A., Güida Raúl Viña and Graciela Punte, *J. Phys. Chem. Solids*, 2015; **81**: 57-65.

[7] Serre C.M., Papillard M., Chavassieux P., Voegel J.C. and Boivin J., *J. Biomed. Mater. Res.*, 1998; **42**: 626-633. DOI 10.1002/(SICI)1097-4636.

[8] Paluszkiewicz C., Slosarczyk A., Pijocha D., Sitarz M., Bucko M., Zima A., Chroscicka A. and Lewandowska-

Szumiel M., *J. Mol. Struct.*, 2010; **976**: 301-309. DOI 10.1016/j.molstruc.2010.04.001.

[9] Grandjean-Laquerrier A., Laquerriere P., Jallot E., Nedelec J.M., Guenounou M., Laurent-Maquin D. and Phillips T.M., *Biomaterials*, 2006; **27**: 3195-3200. DOI 10.1016/j.biomaterials.2006.01.024.

[10] Zhao J., Zhu Y.J., Cheng G.F., Ruan Y.J., Sun T.W., Chen F., Wu J., Zhao X.Y. and Ding G.J., *Mater. Lett.*, 2014; **124**: 208-211. DOI 10.1016/j.matlet.2014.03.054.

[11] Guo X., Yan H., Zhao S., Zhang L., Li Y. and Liang X., *Adv. Powder Technol.*, 2013; **24**: 1034-1038. DOI 10.1016/j.apt.2013.03.002.

[12] Lim H.N., Kassim A. and Huang N.M., *Sains Malaysiana*, 2010; **39**: 267-273.

[13] Deng Y., Wang H., Zhang L., Li Y. and Wei S., *Mater. Lett.*, 2013; **104**: 8-12. DOI 10.1016/j.matlet.2013.03.145.

[14] Mahmoodi S., Ehsani M.R. and Ghoreishi S.M., *J. Ind. Eng. Chem.*, 2010; **16**: 923-928. DOI 10.1016/j.jiec.2010.09.007.

[15] Del Aio E., Gaona D., Hernández-Garrido J.C., Calvino J.J., Basallote M.G., Fernández-Trujillo M.J, Pírez-Omil J.A. and Gatica J.M., *J. Catal.*, 2014; **318**: 119-127. DOI 10.1016/j.jcat.2014.07.001.

[16] Eschemann T.O., Bitter J.H. and de Jong K.P., *Catal. Today*, 2014; **228**: 89-95. DOI 10.1016/j.cattod.2013.10.041.

[17] Sung Y.M., Lee J.C. and Yang J.W., *J. Cryst. Growth*, 2004; **262**: 467-472. DOI 10.1016/j.jcrysgro.2003.10.001.

[18] Kulawong S., Prayoonpokarach S., Neramittagapong A. and Wittayakun J., *J. Ind. Eng. Chem.*, 2011; **17**: 346-351. DOI 10.1016/j.jiec.2011.02.037.

[19] Uysal I., Severcan F. and Evis Z., *Adv. Appl. Ceram.*, 2013; **112**: 149-157. DOI 10.1179/1743676112Y.0000000053.

[20] Kulanthaivel S., Roy B., Agarwal T., Giri S., Pramanik K., Pal K., Ray S.S., Maiti T.K. and Banerjee I., *Mater. Sci. Eng. C*, 2016; **58**: 648-658. DOI 10.1016/j.msec.2015.08.052.

[21] Gozalian A., Behnamghader A., Daliri M. and Moshkforoush A., *Scientia Iranica F.*, 2011; **18**: 1614-1622. DOI 10.1016/j.scient.2011.11.014.

[22] Sutha S., Kavitha K., Karunakaran G. and Rajendran V., *Mater. Sci. Eng. C*, 2013; **33**: 4046-4054. DOI 10.1016/j.msec.2013.05.047.

[23] Bigi A., Fini M., Bracci B., Boanini E., Torricelli P., Giavaresi G., Aldini N.N., Facchini A., Sbaiz F. and Giardino R., *Biomaterials*, 2008; **29**: 1730-1736. DOI 10.1016/j.biomaterials.2007.12.011.

[24] Biggemann D., Prado da Silva M.H., Rossi A.M. and Ramirez A., *Microsc. Microanal.*, 2008; **14**: 433-438. DOI 10.1017/S1431927608080744.

[25] Batra U., Kapoor S. and Sharma., *J. Mater. Eng. Perform.*, 2013; **22**: 1798-1806. DOI 10.1007/s11665-012-0462-2.

[26] Tkalčec E., Popović J., Orlić S., Milardović S. and Ivanković H., *Mater. Sci. Eng. C*, 2014; **42**: 578-586. DOI 10.1016/j.msec.2014.05.079.

[27] Kim Y.G., Seo D.S. and Lee J.K., *J. Phys. Chem. Solids.*, 2008; **69**: 1556-1559. DOI 10.1016/j.msec.2014.05.079.

[28] Zhang H.B., Zhou K.C., Li Z.Y. and Huang S.P., *J. Phys. Chem. Solids*, 2009; **70**: 243-248. DOI 10.1016/j.msec.2014.05.079.

[29] Mishra V.K., Bhattacharjee B.N., Parkash O., Kumar D. and Rai S.B., *J. Alloy Compd.*,

2014; **614**: 283-288. DOI 10.1016/j.jallcom.2014.06.082.

[30] Alshemary A.Z., Akram M., Goh Y.F., Kadir M.R.A., Abdolahi A. and Hussain R., *J. Alloy Compd.*, 2015; **645**: 478-486. DOI 10.1016/j.jallcom.2015.05.064.

[31] Takarroumt N., Kacimi M., Verduraz F.B., Liotta L.F. and Ziyad M., *J. Mol. Catal. A: Chem.*, 2013; **377**: 42-50. DOI 10.1016/j.molcata.2013.04.017.

[32] Boucetta C., Kacimi M., Ensuque A., Piquemal J.Y., Verduraz F.B., Ziyad M., *Appl. Catal. A: Gen.*, 2009; **356**: 201-210. DOI 10.1016/j.apcata.2009.01.005.

[33] Tanaka H. and Ohnishi A., *Adv. Powder Technol.*, 2013; **24**: 1028-1033. DOI 10.1016/j.apt.2013.02.012.